

## OPTICAL-TURBULENCE AND WIND PROFILES AT SAN PEDRO MÁRTIR WITH G-SCIDAR

R. Avila,<sup>1</sup> L. J. Sánchez,<sup>2</sup> F. Ibañez,<sup>1</sup> J. Vernin,<sup>3</sup> E. Masciadri,<sup>2,4</sup> M. Azouit,<sup>3</sup> A. Agabi,<sup>3</sup> and S. Cuevas<sup>2</sup>

### RESUMEN

Se presentan resultados del monitoreo de perfiles de turbulencia óptica en San Pedro Mártir, México, durante 11 noches en abril–mayo 1997 y 16 noches en mayo 2000. La velocidad de las capas turbulentas también se monitoreo, pero sólo durante la temporada del 2000. 6414 perfiles de turbulencia y 3016 perfiles de velocidad fueron medidos y analizados estadísticamente. Los resultados referentes a los perfiles de turbulencia son: (i) el *seeing* producido en los primeros 1.2 km, sin incluir la turbulencia de cúpula, en los telescopios de 1.5 y 2.1 m tiene medianas de 0''63 y 0''44. (ii) La turbulencia por encima de 1.2 km y en la atmósfera completa produce *seeing* con valores medianos de 0''38 y 0''71. (iii) El ángulo de isoplanatismo para corrección total en óptica adaptativa tiene un valor mediano de 1''87. (iv) La correlación temporal de la intensidad de la turbulencia cae a 50% en períodos de tiempo de 2 y 0.5 horas, aproximadamente, para alturas mayores y menores que 16 km sobre el nivel del mar, respectivamente. (v) El tiempo de decorrelación del ángulo de isoplanatismo tiene un valor estimado de 2 horas. Los resultados referentes a los perfiles de viento son: (vi) No se encuentra correlación significativa entre la intensidad de turbulencia ( $C_N^2$ ) y la velocidad de las capas turbulentas. (vii) Las capas por debajo de 5 km y por arriba de 16 km, sobre el nivel del mar, son similarmente lentas, con velocidades medianas de 8.6 y 9.6 m s<sup>-1</sup>. (viii) Entre 9 y 16 km, donde algunas noches tiene lugar la corriente de chorro, la velocidad del viento mediana es de 26.0 m s<sup>-1</sup>. (ix) De las medidas simultáneas de  $C_N^2(h)$  y  $V(h)$ , calculamos el tiempo de coherencia de la turbulencia, capa por capa. Los resultados obtenidos sitúan a San Pedro Mártir entre los sitios más adecuados para la instalación de telescopios ópticos de la próxima generación.

### ABSTRACT

We present the results of monitoring optical-turbulence profiles at the Observatorio Astronómico Nacional de San Pedro Mártir, Mexico, during 11 nights in March and April 1997 and 16 nights in May 2000. The speed of turbulent layers was also monitored, but only for the 2000 period. 6414 turbulence profiles and 3016 wind profiles were measured and statistically analyzed. The main results concerning the turbulence profiles are: (i) the seeing produced by the turbulence in the first 1.2 km at the 1.5-m and the 2.1-m telescopes, not including turbulence inside the domes, has median values of 0''63 and 0''44, respectively. (ii) The median values of the seeing produced above 1.2 km and in the whole atmosphere are 0''38 and 0''71. (iii) The isoplanatic angle for full correction adaptive optics has a median value of 1''87. (iv) The decorrelation time (defined as the time lag for which the temporal correlation drops to 50%) of the turbulence strength at altitudes below and above 16 km above sea level is approximately equal to 2 and 0.5 hours, respectively. (v) The isoplanatic-angle decorrelation-time is estimated to be equal to 2 hours. The results concerning the wind profiles are: (vi) No significant correlation is found between the turbulence intensity ( $C_N^2$ ) and the speed of the turbulent layers  $V$ . (vii) Layers in the first 5 km and higher up than 16 km, above sea level, are similarly slow, with median speeds of 8.6 and 9.6 m s<sup>-1</sup>. (viii) Between 9 and 16 km, where the jet stream takes place in some of the nights, the median wind speed is 26.0 m s<sup>-1</sup>. (ix) From the simultaneous measurements of  $C_N^2(h)$  and  $V(h)$ , we compute the temporal coherence of the turbulence layer by layer. The results obtained here places San Pedro Mártir among the best suited sites for installing next generation optical telescopes.

**Key Words:** ATMOSPHERIC EFFECTS — INSTRUMENTATION: ADAPTIVE OPTICS — SITE TESTING — TURBULENCE

<sup>1</sup>Centro de Radioastronomía y Astrofísica, Universidad Nacional Autónoma de México, Morelia, México (r.avila@astrosmo.unam.mx).

<sup>2</sup>Instituto de Astronomía, Universidad Nacional Autónoma de México, México, 04510 D. F., México.

<sup>3</sup>U.M.R. 6525 Astrophysique, UNSA/CNRS, France.

<sup>4</sup>INAF - Osservatorio Astrofisico di Arcetri, Firenze, Italy.

### 1. INTRODUCTION

The development and operation of ground-based modern astronomical facilities achieving high angular resolution observations, require an increasingly precise characterization of the on site atmo-

spheric turbulence. Fundamental data for such a task are vertical profiles of the optical turbulence, represented by the refractive-index structure constant  $C_N^2(h)$ , and velocity of the turbulent layers  $\mathbf{V}(h)$ . Information about the seeing is necessary but not sufficient. For example, the design of multiconjugate adaptive optics (MCAO) (systems that incorporate several deformable mirrors, each conjugated at a different altitude) requires knowledge of the statistical behavior of the optical-turbulence in the atmosphere like the altitude of the predominant turbulent layers, their temporal variability and the velocity of their displacement. Moreover, the selection of the sites where the next-generation ground-based telescopes are to be installed needs reliable studies of the  $C_N^2$  and  $\mathbf{V}$  profiles at those sites.

These reasons have motivated the accomplishment of two campaigns aimed at monitoring  $C_N^2$  and  $\mathbf{V}$  profiles at the Observatorio Astronómico Nacional de San Pedro Mártir (OAN-SPM). The campaigns took place in 1997 (April and May) and 2000 (May), for a total of 27 nights. Here we present the main results obtained from the  $C_N^2(h)$  and  $\mathbf{V}(h)$  measurements performed during these campaigns. Avila, Vernin, & Cuevas (1998) reported the  $C_N^2(h)$  results from the 1997 observations alone.

Section 2 briefly presents the measurement techniques and the observation campaigns. An overview of the monitored turbulence profiles is given in § 3.1 and the statistical analysis of the  $C_N^2$  vertical distribution is presented in § 3.2. The temporal behavior of  $C_N^2(h)$  is studied in § 3.3. In § 4 the wind profiles and a simple statistical analysis is presented. Finally, § 5 gives a summary of the results.

## 2. MEASUREMENTS OF $C_N^2$ AND $\mathbf{V}$ PROFILES

The principal method followed to measure the turbulence and velocity profiles at the OAN-SPM has been that of the Generalized Scidar (GS). Details of the instrumental concept, together with a complete bibliography, can be found in the web page entitled *Generalized Scidar at UNAM*<sup>5</sup>. Here we give a very succinct description of the instrument and data reduction procedure. We used the GS developed by Vernin's group at Nice University (Avila, Vernin, & Masciadri 1997).

The instrumental concept for the determination of  $C_N^2(h)$  consists in the measurement of the spatial autocorrelation of 1000 to 2000 double-star scintillation-images detected on a virtual plane a few kilometers below the ground. For the determination of the turbulence-layer velocity  $\mathbf{V}(h)$ , the cross-

TABLE 1  
DOUBLE STARS USED FOR THE  
GENERALIZED SCIDAR

Name	$\alpha_{2000}$ <sup>a</sup>	$\delta_{2000}$ <sup>a</sup>	$m_1$ <sup>b</sup>	$m_2$ <sup>b</sup>	$\rho$ (") <sup>c</sup>
Castor	7h34	31°53	1.9	3.0	4.0
$\gamma$ Leo	10h20	19°50	2.3	3.6	4.5
$\zeta$ Uma	13h24	54°56	2.2	3.8	14.4
$\delta$ Ser	15h35	10°32	4.2	5.1	4.0
$\zeta$ Cbr	15h39	36°38	5.0	5.9	6.4
95 Her	18h01	21°36	4.8	5.2	6.3

<sup>a</sup>Right ascension ( $\alpha_{2000}$ ) and Declination ( $\delta_{2000}$ ).

<sup>b</sup>Visible magnitudes of each star.

<sup>c</sup>Angular separation.

correlation of images delayed by 20 and 40 ms is calculated. The exposure time of each image is 1 or 2 ms and the wavelength is centered at 0.5  $\mu\text{m}$ . A pair of 128×128 autocorrelation and cross-correlation maps are saved on disk approximately every 1.2 min. The double stars used as light sources are listed in Table 1. The data shown in this table were obtained from the Washington Double Star Catalog (Mason, Wycoff, & Hartkopf 2002). Many of the sources are multiple systems, but in every case our instrument is only sensitive to the primary and secondary components. Using a maximum entropy algorithm, one  $C_N^2$  profile is retrieved from each autocorrelation. The data reduction of the cross-correlations is performed using an interactive algorithm (Avila, Vernin, & Sánchez 2001). In some cases, the autocorrelation and cross-correlation maps show diagonal bands parallel to each other. These are produced by video noise on the scintillation images. In such cases, the maps pass through a filter that eliminates the bands prior to the data reduction. When the noise is still present after filtering, the maps are rejected. The vertical resolution of each  $C_N^2$  profile depends on the star separation and the zenith angle. All the profiles were re-sampled to an altitude resolution of 500 m.

### 2.1. 1997 Campaign

In the 1997 observing campaign, the GS was installed on the 1.5-m and 2.1-m telescopes (1.5-mT and 2.1-mT) for 8 and 3 nights respectively (1997 March 23–30 and April 20–22 UT). Simultaneously, the IA-UNAM differential image motion monitor (DIMM) (Sarazin & Roddier 1990) was used to measure the open air seeing. The 2.1-mT is installed on top of a 15 meter tall building lying at the summit of

<sup>5</sup><http://www.astrosmo.unam.mx/~r.avila/Scidar>

the mountain (2850 m above sea level) in such a way that no obstacle can generate ground turbulence. On the other hand, the 1.5-mT is constructed closer to the ground level, on a site located below the summit.

### 2.2. 2000 Campaign

The 2000 campaign took place in May 7 through 22, UT. A number of instruments were deployed:

- **The GS**, installed during 9 and 7 nights (7–15 and 16–22 April UT) on the 1.5-mT and 2.1-mT telescopes, respectively.
- **Instrumented balloons**, launched to sense one detailed  $C_N^2$  profile per night. The balloon launches require quiet wind conditions or a large area clear of obstacles in case of windy conditions. Trees and buildings of the observatory site prevented us from launching balloons when the wind was strong. In these cases, balloons were launched from Vallecitos, an area clear of trees, 3 km away from the observatory and 300 m below.
- **A 15m-high mast**, equipped with microthermal sensors —of the same kind as those used on the balloons— to measure the  $C_N^2$  values at 7 different altitudes up to 15 m (Sánchez et al. 2004).
- **A DIMM**, installed 8 m away from the mast, to monitor the open air seeing.
- **Meteorological balloons**, to measure the profiles of  $T$ ,  $P$ ,  $\mathbf{V}$ , and the humidity  $q$ . These were launched from Colonet, a town on the Pacific Ocean shore.

The measurements obtained with the mast and the DIMM led to a study of the contribution of the surface layer to the seeing (Sánchez et al. 2004).

Most of the data gathered in this campaign were used for the calibration of the Meso-NH atmospheric model for the 3D simulation of  $C_N^2$  (Masciadri, Avila, & Sánchez 2004).

## 3. $C_N^2(h)$ PROFILES

### 3.1. $C_N^2(h)$ Data Overview

The number of turbulence profiles measured in the 1997 and the 2000 campaigns are 3398 and 3016, making a total of 6414 estimations of  $C_N^2(h)$ . Figure 1 shows most of the  $C_N^2$  profiles obtained during the 2000 campaign. The aim of this figure is to give the reader a feeling of the evolution of the turbulence profiles during each night and from night to night. The three upper rows correspond to the data obtained with the 1.5-mT. In the two last rows, the data obtained with the 2.1-mT is represented.

The first 2.1-mT night was cloudy. The blank zones correspond to either technical problems, clouds or changes of source.  $C_N^2$  values for altitudes within the observatory and 1 km lower are to be taken as part of the response of the instrument to turbulence at the observatory level. For altitudes lower than that, the  $C_N^2$  values are artifacts of the inversion procedure, and should be ignored.

Generally, the most intense turbulence is located at the observatory level, where the contributions from inside and outside of the telescope dome are added. In the statistical analysis, presented in § 3.2, dome turbulence is subtracted. The profiles obtained with the 2.1-mT show a fairly stable and strong layer between 10 and 15 km, corresponding to the tropopause (as deduced from the balloon data). This layer is rarely present in the data obtained with the 1.5-mT. Sporadic turbulence bursts are noticed at altitudes higher than 15 km.

### 3.2. Statistics on the $C_N^2$ vertical-distribution

#### 3.2.1. Dome seeing

All the “raw”  $C_N^2$  profiles, as those shown in Figure 1, include in the ground layer the turbulence inside the telescope dome. For the characterization of the site, we need to remove the dome seeing contribution from the profiles. The method followed to estimate the dome  $C_N^2$  is explained in detail by Avila et al. (2001) and some improvements are suggested by Masciadri, Avila, & Sánchez (2002)XX. The dome seeing was determined for 84% of the profiles measured during the 2000 campaign. In the remaining 16% of the profiles, the determination of the dome seeing was “ambiguous”, so we did not include these data to the dome seeing database. Refer to Avila et al. (2001) for a precise definition of an “ambiguous” determination of the dome seeing.

Figure 2 represents the cumulative distribution functions of the dome-seeing values obtained. Table 2 gives the median values, 1st and 3rd quartiles. The optical turbulence inside the 1.5-mT is substantially higher than that in the 2.1-mT. Note that neither cumulative distribution is symmetrical with respect to the corresponding median value.

In the remaining part of the paper, all the statistical results concerning the turbulence near the ground are free of dome-turbulence.

#### 3.2.2. Median $C_N^2(h)$ profiles

The median, 1st and 3rd quartiles values of  $C_N^2(h)$  obtained with the 1.5-mT and 2.1-mT are represented in Figures 3a and 3b, respectively. These profiles were computed using the data from both

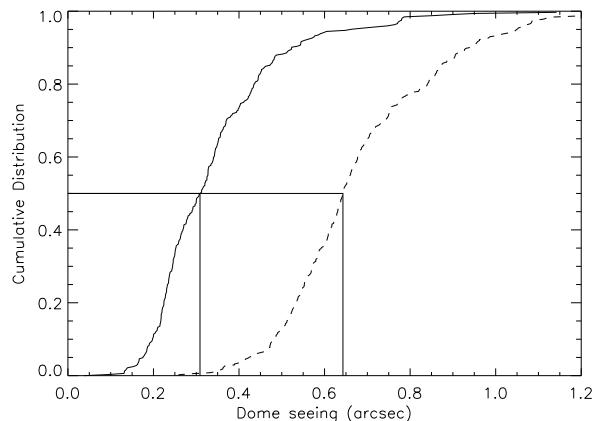


Fig. 2. Cumulative distribution of the seeing generated inside the dome of the 2.1-mT (full line) and the 1.5-mT (dashed line). The vertical and horizontal lines indicate the median values. These values together with the 1st and third quartiles are reported in Table 2.

TABLE 2  
DOME SEEING STATISTICS

Tel.	1st Quartile (arcsec)	Median (arcsec)	3rd Quartile (arcsec)
1.5-mT	0.55	0.64	0.77
2.1-mT	0.23	0.31	0.41

campaigns, i.e., the complete GS data set, with the dome seeing removed. The most important characteristic is that the turbulence measured at the telescope level is notably more intense at the 1.5-mT than at the 2.1-mT. We believe that this is mainly due to the fact that the 1.5-mT is located at ground level, while the 2.1-mT is installed on top of a 20-m building. Moreover, the 2.1-mT building is situated at the observatory summit whereas the 1.5-mT is located at a lower altitude. Figure 3c shows the median profile calculated from all the  $C_N^2$  profiles measured with the GS in the OAN-SPM (i.e., both campaigns).

Another difference seen in the median profiles obtained with the 1.5-mT and 2.1-mT (Figures 3a and 3b) is that the tropopause layer, which is centered at 12 km approximately, is much stronger on Figure 3b than on Figure 3a. This is not a consequence of the telescope which was used. By chance, it happened that while observing with the 1.5-mT during the 2000 campaign the turbulence at that altitude — and everywhere higher than 8 km — was very weak,

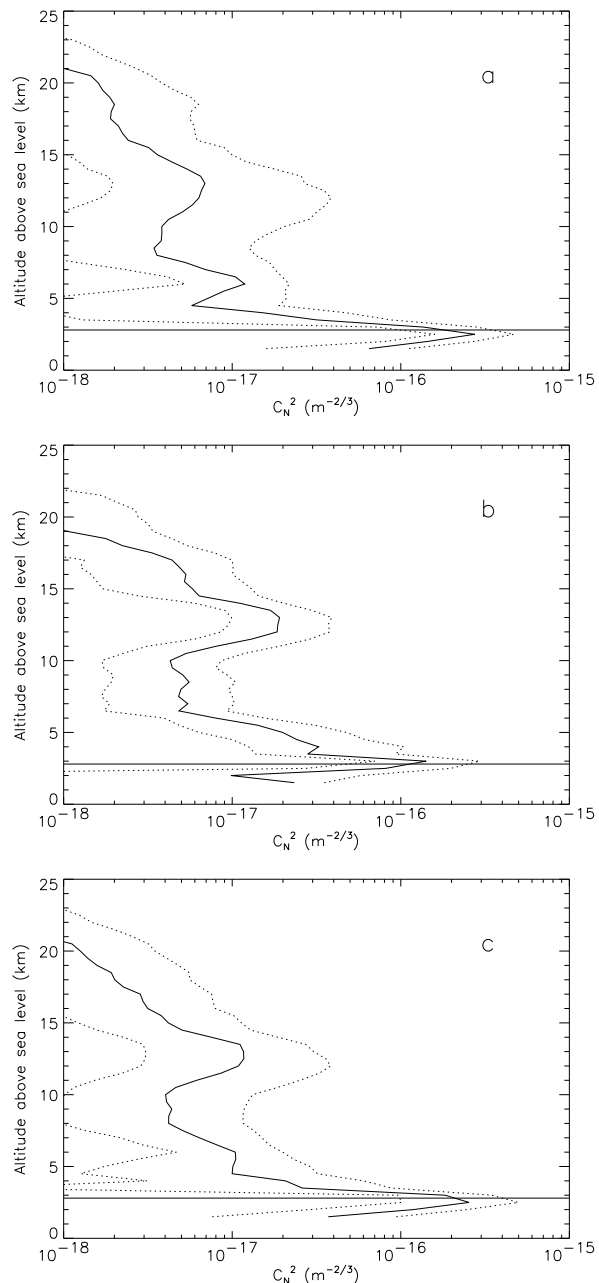


Fig. 3. Median (full line), 1st and 3rd quartiles (dashed lines) of the  $C_N^2(h)$  values obtained with the GS at the (a) 1.5-mT, (b) 2.1-mT and (c) both telescopes, during 1997 and 2000 campaigns. The horizontal axis represents  $C_N^2$  values, in logarithmic scale, and the vertical axis represents the altitude above sea level. The horizontal lines indicate the observatory altitude. Dome seeing has been removed.

as seen on Figure 4. During that campaign, between the 1.5-mT and 2.1-mT observations, there was one cloudy night. In contrast with the first 9 nights of

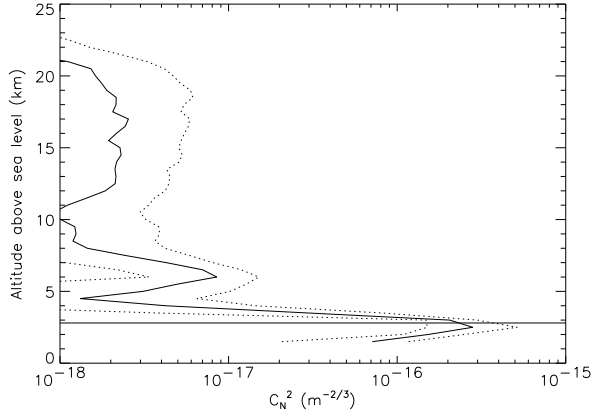


Fig. 4. Similar to Figure 3 but for the GS profiles obtained at the 1.5-mT during the 2000 campaign.

the campaign (when the GS was installed on the 1.5-mT), during the first observable night on the 2.1-mT, the turbulence in the tropopause was extremely intense. This can be seen on the first box of the 4th row of Figure 1. It is generally believed that the turbulence intensity at the tropopause is strong due to a dramatic increase of the overall vertical gradient of the potential temperature and the commonly high-velocity wind (jet stream) in that zone of the atmosphere. However, new evidence that contradicts this speculation—or at least that suggests a more complicated phenomenon—is emerging, which motivates a deeper investigation. A first step could be to gather a more complete statistical data set. For the moment, we note that 32% of the profiles measured at the OAN-SPM do not show a significant optical turbulence at the tropopause.

### 3.2.3. Seeing for different atmospheric slabs

From a visual examination of Figure 1, we can determine five altitude slabs that contain the predominant turbulent layers. These are [2;4], [4;9], [9;16], [16;21] and [21;25] km above sea level. In each altitude interval of the form  $[h_l;h_u]$  (where the subscripts  $l$  and  $u$  stand for “lower” and “upper” limits) and for each profile, we calculate the turbulence factor

$$J_{h_l;h_u} = \int_{h_l}^{h_u} dh C_N^2(h) \quad , \quad (1)$$

and the correspondent seeing in arc seconds:

$$\epsilon_{h_l;h_u} = 1.08 \times 10^6 \lambda^{-1/5} J_{h_l;h_u}^{3/5} \quad . \quad (2)$$

For the turbulence factor corresponding to the ground layer,  $J_{2;4}$ , the integral begins at 2 km in order to include the complete  $C_N^2$  peak that is due

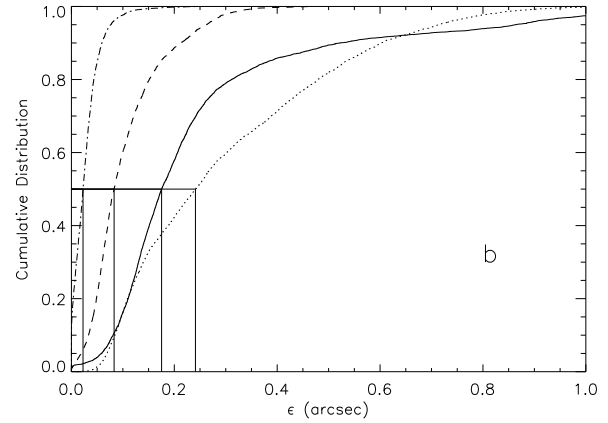
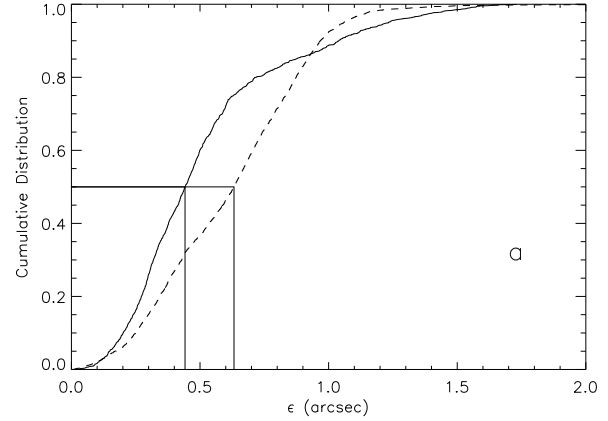


Fig. 5. Cumulative distributions of the seeing generated in different atmosphere slabs: (a) [2;4] km for the 2.1-mT (full line) and the 1.5-mT (dashed line) without dome seeing; (b) [4;9] km (full line), [9;16] km (dotted line), [16;21] km (dashed line), [21;25] km (dash-dotted line). The horizontal and vertical lines indicate the median values, which are reported in Table 3.

to turbulence at ground level (2.8 km). Moreover,  $J_{2;4}$  does not include dome turbulence. The seeing values have been calculated for  $\lambda = 0.5 \mu\text{m}$ . In Figure 5a the cumulative distribution functions of  $\epsilon_{2;4}$  obtained at the 1.5-mT and the 2.1-mT, calculated using the complete data set, are shown. As discussed in § 3.2.2, the turbulence at ground level at the 1.5-mT is higher than that at the 2.1-mT. The cumulative distributions of the seeing originated in the four slabs of the free atmosphere (from 4 to 25 km) are represented in Figure 5b. The strongest turbulence is encountered from 9 to 16 km, where the tropopause layer is located. The turbulence at altitudes higher than 16 km is fairly weak, which is a fortunate feature for the use of adaptive optics (AO), because it tends to increase the corrected field-of-view. Finally, Figures 6a and 6b show the cumulative distribution

TABLE 3  
SEEING STATISTICS FOR DIFFERENT  
ATMOSPHERE SLABS (arcsec)

Slab (km)	1st Q <sup>a</sup> (arcsec)	Median (arcsec)	3rd Q <sup>a</sup> (arcsec)
[2; 4] @ 2.1-mT <sup>b</sup>	0.30	0.44	0.63
[2; 4] @ 1.5-mT <sup>b</sup>	0.38	0.63	0.83
[4; 9]	0.12	0.17	0.27
[9; 16]	0.12	0.24	0.43
[16; 21]	0.05	0.08	0.14
[21; 25]	0.01	0.02	0.04
[2; 25] <sup>c</sup>	0.52	0.71	0.99

<sup>a</sup>1st and 3rd quartiles.

<sup>b</sup>Without dome seeing.

<sup>c</sup>As if measured at the 2.1-mT and without dome seeing (see text).

of the seeing produced in the free atmosphere,  $\epsilon_{4;25}$ , and in the whole atmosphere,  $\epsilon_{2;25}$ , respectively. The computation of  $\epsilon_{2;25}$  is performed as follows: for each profile of the complete data set (both campaigns and both telescopes) we calculate  $J_{4;25}$  and add a random number that follows the same log-normal distribution as that of  $J_{2;4}$  obtained in for the 2.1-mT. Then the corresponding seeing value is calculated using Equation 2. This way, we obtain a distribution of  $\epsilon_{2;25}$  values as if they were measured using the 2.1-mT. The reason for doing so, is that the values of  $\epsilon_{2;25}$  that we obtain are more representative of the site potentialities than if we had used the distribution of  $J_{2;4}$  obtained for the 1.5-mT. The median values of all the cumulative distributions presented in this Section are reported in Table 3.

### 3.3. Temporal Autocorrelation of $C_N^2(h)$

What are the characteristic temporal scales of the fluctuations of optical turbulence at different altitudes in the atmosphere? This question has been of interest for a long time, and mostly in recent years, as the development of Multiconjugate Adaptive Optics (MCAO) require knowledge of the properties of the optical turbulence in a number of slabs in the atmosphere. Racine (1996) studied the temporal fluctuations of free atmosphere seeing above Mauna Kea. He computed the seeing values by integrating turbulence profiles measured in 1987 by Vernin's group from Nice University using the scidar technique. The  $C_N^2$  profiles did not include the turbulence from the

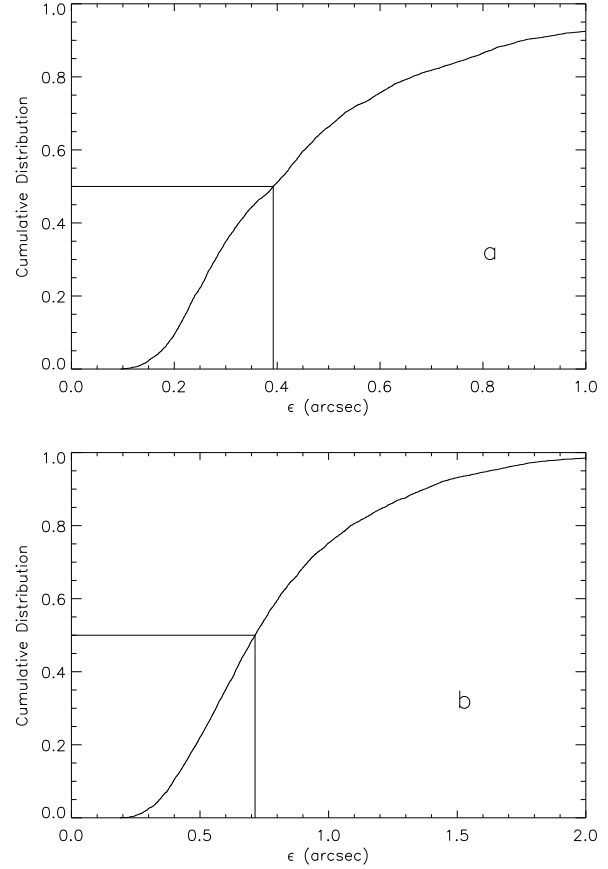


Fig. 6. Cumulative distributions of the seeing generated in (a) the free atmosphere (altitude higher than 4 km),  $\epsilon_{4;25}$ , and (b) the whole atmosphere,  $\epsilon_{2;25}$ , without dome seeing (see text for details). The horizontal and vertical lines indicate the median values, which are reported in Table 3.

first kilometer, because the classical mode of the scidar was employed, as the generalized mode did not exist at that time. Muñoz-Tuñón, Varela, & Vernin (1992) used DIMM data to study the temporal behavior of the open-air seeing at Roque de Los Muchachos observatory. Finally, Tokovinin, Baumont, & Vasquez (2003) presented the temporal autocorrelation of the turbulence factor in three representative slabs of the atmosphere above Cerro Tololo Inter-American Observatory, using data obtained with the recently developed Multi-Aperture Scintillation Sensor, which provides  $C_N^2$  measurements at six altitudes in the atmosphere.

In this Section we investigate the temporal autocorrelation of the turbulence factors  $J_{h_l;h_u}$ , for the five slabs introduced in § 3.2.3.

### 3.3.1. Methodology

The process of building the appropriate sequences of  $J_{h_l;h_u}(t_i)$  values is explained below: Typically, three stars are used as light sources each night, in a sequence such that the zenith angle never exceeds  $\sim 40^\circ$ . When changing from one star to the following, the region of the atmosphere that is sensed by the instrument changes significantly and so  $C_N^2(h)$  can also change, as shown by Masciadri et al. (2002). To avoid the confusion between a temporal and a spatial variation of  $J_{h_l;h_u}$ , the sequences  $J_{h_l;h_u}(t_i)$  never include data obtained with two different stars. From the 2000-campaign data, we built 35 sequences  $J_{h_l;h_u}(t_i)$  for each of the five altitude intervals. The temporal sampling of the turbulence profiles depends on the number of scintillation images recorded for the computation of each profile, which in turn depends on the source magnitude. Consequently, each sequence  $J_{h_l;h_u}(t_i)$  is re-sampled with a regular time-interval of  $\delta t = 1.14$  minutes, which is the mean temporal sampling of the  $C_N^2$  profiles. Moreover, while observing a given source, the data acquisition may be interrupted. If the interruption is longer than  $2\delta t$ , then the temporal gap is filled with zero values for  $J_{h_l;h_u}(t_i)$ .

For each altitude interval, the calculation of the temporal autocorrelation, as a function of the temporal lag  $\Delta t$ , is performed as follows: For each  $J_{h_l;h_u}$  sequence labeled  $s$ , we first compute

$$C_s(\Delta t) = \sum_{i=1}^{N_{\Delta t,s}} (J_s(t_i) - \overline{J_s}) (J_s(t_i + \Delta t) - \overline{J_s}) \quad , \quad (3)$$

where the product is set equal to zero if either  $J_s(t_i) = 0$  or  $J_s(t_i + \Delta t) = 0$ .  $\overline{J_s}$  is the mean of the nonzero values of  $J_s(t_i)$ , and  $N_{\Delta t,s}$  is the number of computed nonzero products, which depends on  $\Delta t$  and the number of nonzero values of  $J_s(t_i)$  in the sequence  $s$ , and is calculated numerically. The autocorrelation for each altitude slab is then given by

$$\Gamma(\Delta t) = \frac{A(\Delta t)}{B} \quad , \quad \text{where} \quad (4)$$

$$A(\Delta t) = \frac{1}{N_{\Delta t}} \sum_{s=1}^{N_s} C_s(\Delta t) \quad , \quad (5)$$

$$B = \frac{1}{N_0} \sum_{s=1}^{N_s} C_s(0) \quad \text{and} \quad (6)$$

$$N_{\Delta t} = \sum_{s=1}^{N_s} N_{\Delta t,s} \quad . \quad (7)$$

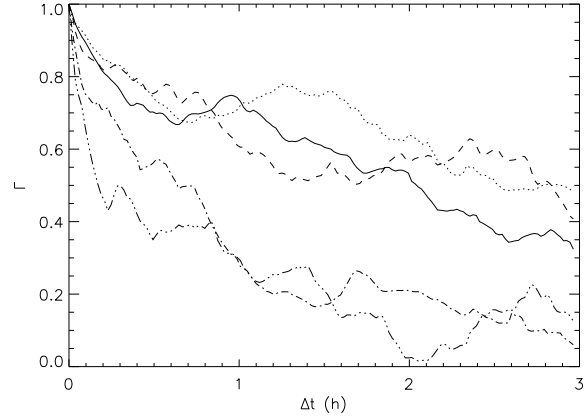


Fig. 7. Temporal autocorrelation of the turbulence factor  $J_{h_l;h_u}(t_i)$ , for intervals  $[h_l;h_u]$  equal to [2;4] (full line), [4;9] (dotted line), [9;16] (dashed line), [16;21] (dash-dotted line) and [21;25] (dash-dot-dotted line) km.

$N_s$  is the number of sequences for each altitude interval. From the definitions of  $C_s(\Delta t)$  and  $N_{\Delta t}$  (Equations 3 and 7), it can be noticed that the normalization factor  $B$  only takes into account nonzero values of  $J_s(t_i)$ .

### 3.3.2. Results

The temporal autocorrelations for the five atmosphere slabs were computed using the 2000-campaign data set. The turbulence inside the dome was removed. The number  $N_{\Delta t}$  of products summed to calculate  $\Gamma(\Delta t)$  range from  $\sim 2902$  for  $\Delta t = 0$  to  $\sim 870$  for  $\Delta t = 3$  hrs. The results are shown in Figure 7. For every slab, the autocorrelation shows a steep descent for short temporal lags followed by a less rapid decrease for longer lags. It can be seen that in the first three altitude slabs the turbulence de-correlate more slowly than in the two higher slabs. The time lags for a 50% decorrelation are approximately 2, 2.5, 1.7, 0.7 and 0.2 hours in the altitude ranges [2;4], [4;9], [9;16], [16;21] and [21;25] km, respectively. The turbulence in the highest slab is so weak (as seen in Figure 5), that  $\Gamma(\Delta t)$  for that slab might be strongly affected by the noise variations. Turbulence in the highest layers evolve more rapidly than in the lower layers but introduces less distortions in the wavefront because they are weaker. In the altitude ranges [2;4] and [9;16] km the turbulence is the most intense, but fortunately, the variations are slow.

## 4. WIND PROFILES

### 4.1. $\mathbf{V}(h)$ Data Overview

We have been able to retrieve 3016 profiles from this observation campaign. Figure 8 shows a mosaic

view of all the wind-speed profiles. It can be seen that at the observatory level, the wind is generally weak. As we have excluded the data corresponding to the dome seeing, wind values at ground level are associated to open-air turbulence.

In many cases, dots with different colors appear superimposed, which indicates the presence of several turbulent layers with altitude differences smaller than the vertical resolution of the  $C_N^2$  profiles, but with detectable velocity differences. This feature constitutes a strong advantage of the simultaneous measurement of  $C_N^2(h)$  and  $\mathbf{V}(h)$  as opposed to the solely measurement of  $C_N^2(h)$ . The velocity of the layers represents an additional dimension in the parameter space that characterizes each layer. Therefore, the determination of each layer velocity can help to identify individual turbulent layers.

The fastest turbulent layers are found between 9 and 16 km. In this altitude range, a slow modulation of the layer speed from night to night can be noticed: during the first four nights the speed was lower than  $20 \text{ m s}^{-1}$ , then it started to increase, reaching  $55 \text{ m s}^{-1}$  on May 17 UT, and then decreased to values lower than  $10 \text{ m s}^{-1}$  on the last was generally lower than  $10 \text{ m s}^{-1}$ .

From a visual inspection of Figures 1 and 2, it can be seen that only the night on May 17 UT and in the jet stream layer, an evident correlation is present between  $C_N^2$  and speed values. This is confirmed by Figure 9, where the  $C_N^2$  values are plotted against the layer speed, for each layer detected in the whole campaign. Each frame corresponds to a different altitude interval. No particular correlation between the  $\mathbf{V}$  and  $C_N^2$  values is noticed, apart from the layers in the 9 to 16 km (Figure 9c) range having speeds higher than  $50 \text{ m s}^{-1}$ , which have particularly intense turbulence ( $C_N^2 \gtrsim 5 \times 10^{-17} \text{ m}^{-2/3}$ ). Although this behavior is evident in our data set, further measurements would be required to draw a general conclusion. The observed general lack of correlation between  $C_N^2$  and  $\mathbf{V}$  might be due to the fact that the optical turbulence is triggered by vertical instabilities that take place at scales much smaller than the altitude resolution of the  $C_N^2$  profiles obtained with the GS.

#### 4.2. Wind Speed Profile Statistics

Using all the measured  $\mathbf{V}$  profiles, we have computed the median, first and third quartiles values of the layer speed  $V$  as a function of height. We recall that the first quartile, median and third quartile,  $q_1$ ,  $q_2$  and  $q_3$  of a distribution, are such that 25, 50 and 75% of the events have values lower than  $q_1$ ,  $q_2$  and

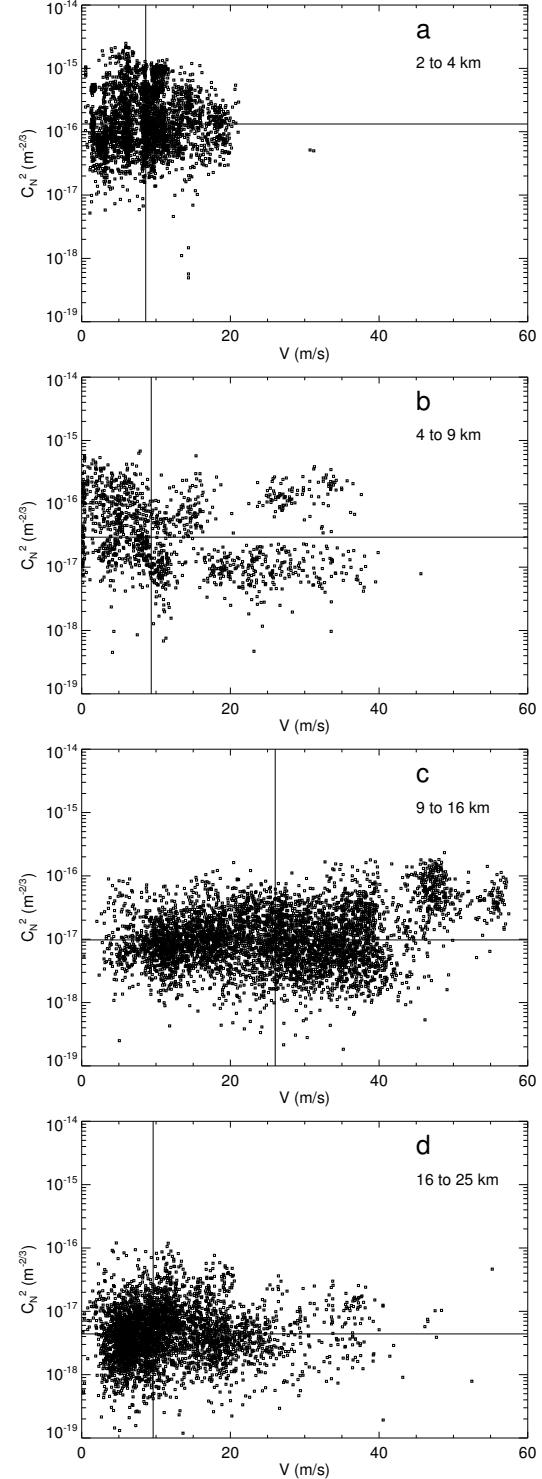


Fig. 9.  $C_N^2$  against  $V$  for all the turbulent layers detected. Each frame corresponds to a different altitude range above sea level, as indicated by the frame labels. The horizontal and vertical lines in each frame indicate the median values of  $C_N^2$  and  $V$ .

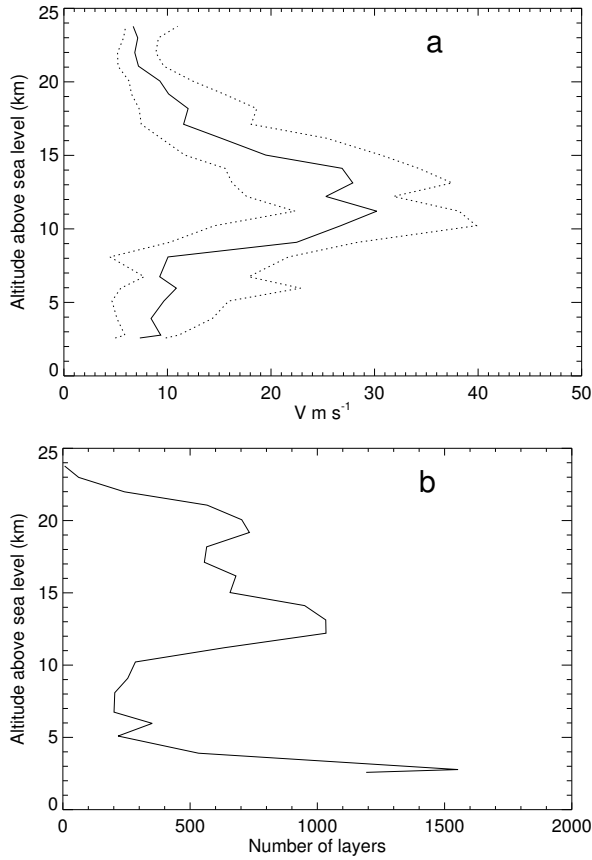


Fig. 10. (a). Profiles of median (solid line), first and third quartiles (dotted lines) of the wind speed. (b) Profile of the number of data used for the statistical calculations. The dome-seeing layer was excluded.

$q_3$ , respectively. The corresponding plots are shown in Figure 10a. It can be seen that the wind speed has similar low values near the ground (within the first 4 km) and above 16 km. In between, which corresponds to the jet stream zone, the wind speed increases strongly. The significance of the statistical values for each altitude is indicated by the number of measurements used in the computation, *i.e.*, the number of detected layers, shown in Figure 10b.

A more complete statistical description of the wind speed values is obtained from their cumulative distribution function (CDF), which corresponds for each value of  $V$ , to the probability of occurrence of such a value or a lower one. We computed one CDF for the wind values grouped in each of four altitude intervals: 2-4, 4-9, 9-16 and 16-25 km above sea level, as shown in Figure 11. We can see, for example, that 10% of the  $V$  values are lower than 3, 2, 10 and 5  $m s^{-1}$  in the 2-4, 4-9, 9-16 and 16-25 km slabs, respectively, and 10% of the values are higher than 15,

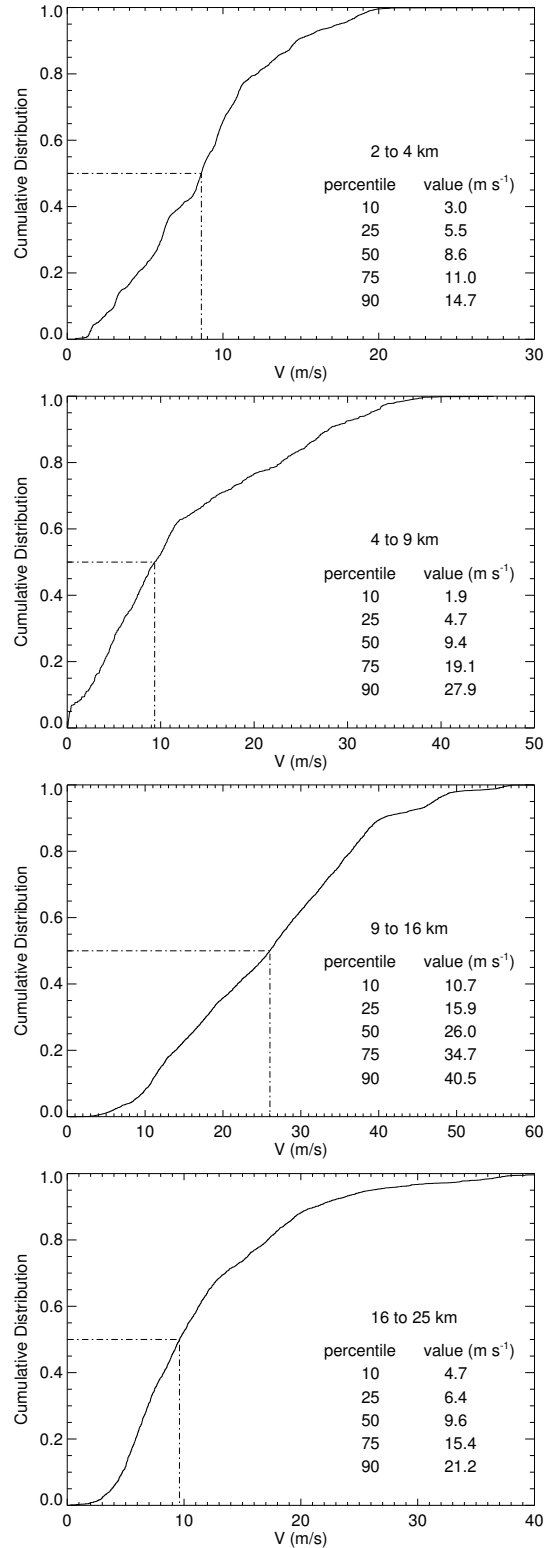


Fig. 11. Cumulative distribution of the wind values in the altitude ranges indicated in each plot. The dome-seeing layer was excluded for the 2 to 4 altitude range.

28, 40 and 21 m s<sup>-1</sup>. These numbers characterize the extreme wind conditions at each altitude interval.

#### 4.3. Coherence Time Profiles

From the  $C_N^2$  and  $\mathbf{V}$  values of each detected layer, the coherence time  $\tau$  of the wavefront deformations produced by that layer can be calculated:

$$\tau = 0.31 \frac{r_{0\text{ind}}}{V}, \quad (8)$$

where  $r_{0\text{ind}}$  corresponds to the Fried's parameter that would occur if only the given layer was present:

$$r_{0\text{ind}} = \left[ 0.423 \left( \frac{2\pi}{\lambda} \right)^2 C_N^2 \Delta h \right]^{-3/5}, \quad (9)$$

where the wavelength  $\lambda = 0.5 \mu\text{m}$ . The value of  $\tau$  for a given layer constrains the temporal frequency at which a deformable mirror (DM) should operate if it had to completely compensate the wavefront deformations introduced by that layer. We have calculated  $\tau(h)$  from each  $C_N^2$  and  $\mathbf{V}$  profiles. The median, first and third quartiles of  $\tau(h)$  are shown in Figure 12. From the median  $C_N^2$  profile measured at SPM (Figure 3c), one could envisage a MCAO system constituted of three deformable mirrors conjugated at ground level, 6 km and 13 km above sea level. For such conjugation altitudes, the median value of  $\tau$  would be 38, 25 and 15 ms approximately.

It is interesting to note that the variation of  $\tau$  with altitude, seems to be mainly governed by the variation of  $V$ . This is shown by the reasonably good agreement between the median of  $\tau(h)$ , and the median of the function

$$\tau_*(h) = 0.31 \frac{r_{0\text{med}}}{V(h)}, \quad (10)$$

where  $r_{0\text{med}} = 1.8 \text{ m}$ , is the median value of  $r_{0\text{ind}}$  for all altitudes and all turbulence profiles (we remind that  $r_{0\text{ind}}$  is computed for 500-m slabs). The median profiles of  $\tau(h)$  and  $\tau_*(h)$  are shown in solid and dashed lines, respectively, in Figure 12. The strong dependence of the variation with height of  $\tau$  on that of  $V$  can be explained by the analysis of the derivative of Equation 8:

$$\Delta\tau = 0.31 \frac{\Delta r_{0\text{ind}} \bar{V} - \bar{r}_{0\text{ind}} \Delta V}{\bar{V}^2}. \quad (11)$$

The pertinent comparison here is between the terms  $\Delta r_{0\text{ind}} \bar{V}$  and  $\bar{r}_{0\text{ind}} \Delta V$ . Taking  $\bar{V}$  and  $\bar{r}_{0\text{ind}}$  as the median values of  $V$  and  $r_{0\text{ind}}$ , and  $\Delta V$  and  $\Delta r_{0\text{ind}}$  as the variation with height of the corresponding parameters—that is the standard deviation of the values

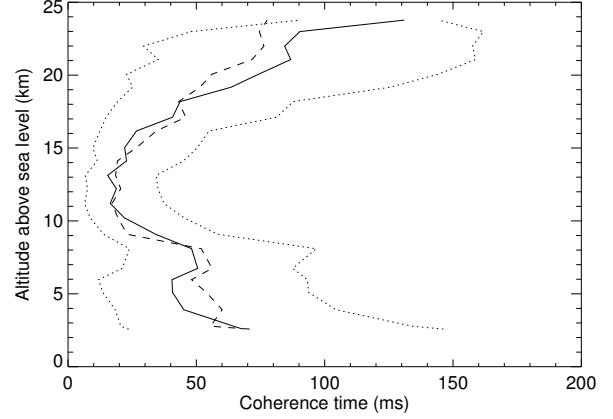


Fig. 12. Median (solid line), first and third quartiles (dotted lines) profiles of the coherence time for adaptive optics, as explained in the text (Equations 8 and 9). The dashed line represents the coherence time profile computed using Equation 10.

of the median profiles of  $V$  and  $r_{0\text{ind}}$ — we obtain  $\bar{V} = 10.1 \text{ m s}^{-1}$ ,  $\bar{r}_{0\text{ind}} = 1.8 \text{ m}$ ,  $\Delta V = 8.1 \text{ m s}^{-1}$  and  $\Delta r_{0\text{ind}} = 0.4 \text{ m}$ . Thus,  $\Delta r_{0\text{ind}} \bar{V} = 4.04$  and  $\bar{r}_{0\text{ind}} \Delta V = 14.58$ , which indicates that  $\Delta V$  has almost 4 times more impact on  $\Delta\tau$  than  $\Delta r_{0\text{ind}}$ .

This is the first time that a study on coherence time profiles,  $\tau$ , is published. It is extremely useful for the development of the next generation of adaptive optics systems.

#### 4.4. Comparison with other measurements and data sets

The goal here is to compare three different values of the wind velocity profiles: those obtained with the GS, the wind speed measured simultaneously from instrumented balloons and the values obtained, for the same nights, from the global circulation model NCEP/NCAR (National Center for Environmental Prediction/National Center for Atmospheric Research) Reanalysis Project. This is the first published comparison between GS and NCEP/NCAR wind profiles.

The balloons used are described by Azouit & Vernin (2005). The wind values are retrieved from the temporal derivative of the balloon horizontal position.

The NCEP/NCAR Reanalysis database model uses a state-of-the-art analysis and forecasting system to perform data assimilation using data from 1948 to the present. It is considered as one of the most reliable analyzed fields (Kisler et al. 2001) as it is constrained by observational information such as land, marine, balloon, satellite and aircraft data.

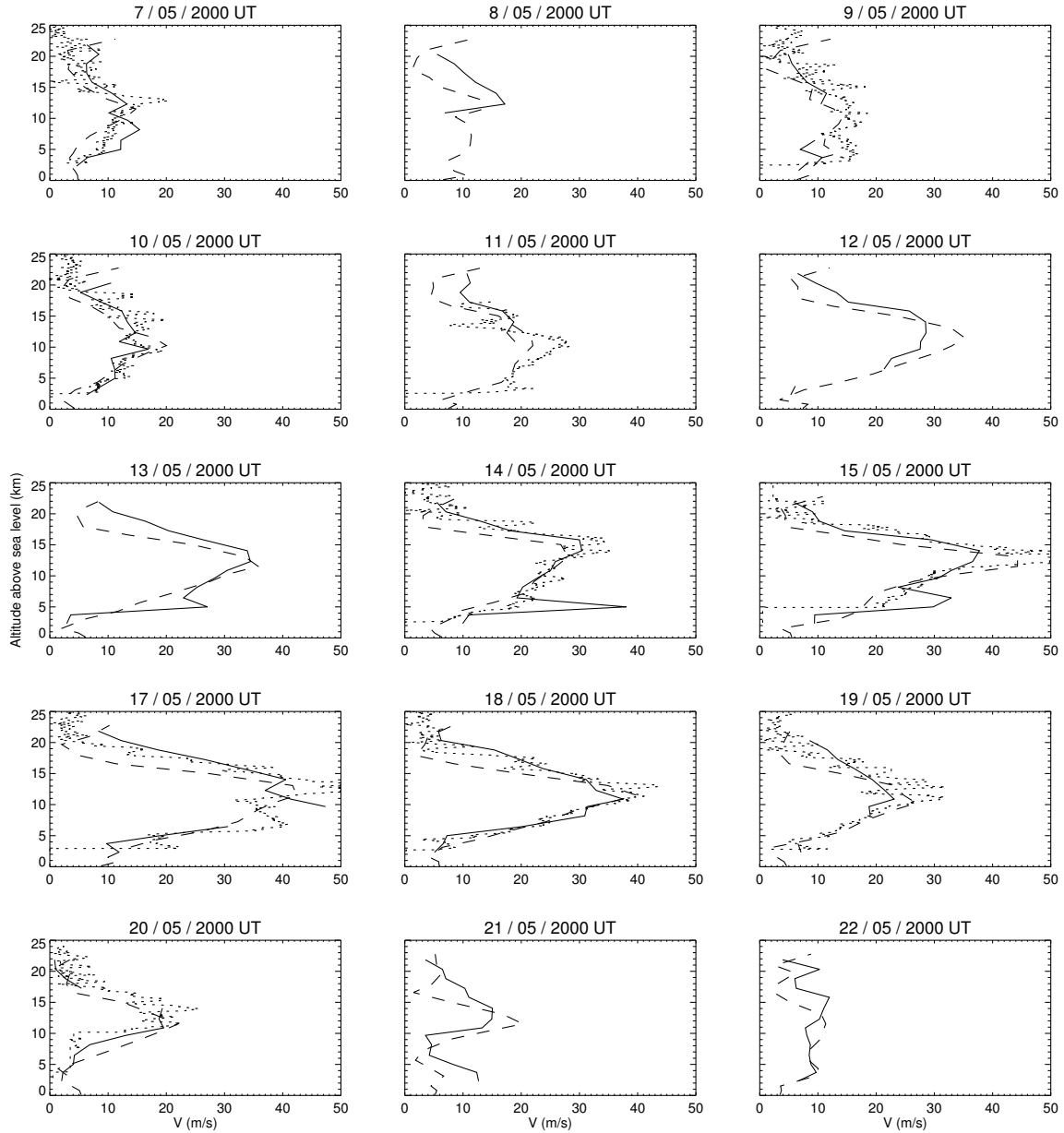


Fig. 13. Similar to Figure 8, but here each frame shows the mean speed profile as measured with the GS (solid lines), wind profiles obtained from the NCEP/NCAR Reanalysis project (dashed lines) and wind profiles measured with balloons (dotted lines). The GS profiles exclude dome turbulence. The NCEP/NCAR Reanalysis project profiles are the average of the 6 and 12 UT data. Each balloon profile corresponds to a single balloon launch. On some nights there was no balloon data.

The Derived NCEP Pressure Level Product provides the 6-hourly U-wind and V-wind components of wind velocity at 17 different pressure levels.

San Pedro Mártir (SPM) geographic coordinate are  $+31^{\circ}05$  latitude and  $-115^{\circ}47$  longitude, while the grid points closest to SPM coordinates are  $+30^{\circ}00$  and  $-115^{\circ}0$ , respectively. We assume a stan-

dard atmosphere to associate the 17 pressure levels to altitudes e.g., 200 mb corresponds to 12 km above sea level. For each altitude, we obtained the velocity module from the  $U$  and  $V$  wind components for the 4 daily forecasted values<sup>6</sup>. For GS comparison pur-

<sup>6</sup>Wind blows to the East and North for  $U > 0$  and  $V > 0$ , respectively.

poses we average only the 6 and 12 UT wind velocity values.

The comparison of the wind speed profiles for 15 nights are shown in Figure 13, where the date is indicated on top of each frame. The solid lines correspond to the mean speed profiles obtained each night with the GS, excluding dome turbulence. The dotted lines are the wind speeds measured with balloons when available. There was at most one balloon flight per night. The wind speed profiles obtained from the NCEP/NCAR Reanalysis model are shown in dashed lines. A visual comparison shows a very good agreement between the three data sets. The NCEP/NCAR Reanalysis profiles reproduce remarkably well the in situ measurements both, those from the instrumented balloons and also the GS values, excepting the GS features shown on May 13, 14 and 15 at about 5 km, which are due to isolated intense wind misdetections, as can be seen in Figure 8. The higher resolution of the balloon measurements shows the spatial wind speed fluctuations that could not be appreciated otherwise.

This cross comparison brings confidence on all three methods for the determination of the wind speed profiles. Particularly, it indicates that for site prospection, it may suffice to determine the wind speed profile from the NCEP/NCAR Reanalysis, rather than actually measure the profiles at a given site. The advantage of the GS measurements, is that they provide the velocity of the turbulence layers themselves, which is what really matters for high angular resolution techniques.

## 5. SUMMARY AND CONCLUSIONS

Turbulence profiles and velocity of the turbulence layers have been monitored at the OAN-SPM, during 11 nights in April–May 1997 and 16 nights in May 2000. The GS was installed at the foci of the 1.5-mT and 2.1-mT. Turbulence inside the dome is detected by the instrument, but for each profile, this contribution has been estimated and separated from the turbulence near the ground outside the dome. The result is a data set consisting of two subsets: turbulence profiles free of dome seeing and dome seeing values. The statistical analysis of this data set lets us draw the following conclusions:

- The turbulence inside the 1.5-mT is much stronger than that at the 2.1-mT, with median values of  $0''.64$  and  $0''.31$ .
- The precise location of each telescope influences the turbulence measured near the ground. The 1.5-mT is installed basically at ground level and lower than the site summit, while the 2.1-mT is

on top of a 20-m building and at the site summit. A consequence of this is that the median values of the seeing produced in the first 1.2 km are  $0''.63$  and  $0''.44$  for the 1.5-mT and 2.1-mT, respectively.

- The seeing generated in the free atmosphere (above 1.2 km from the site), has a median value of  $0''.38$ . This very low value encourages adaptive optics observations, as the lower the turbulence in the higher layers, the broader is the corrected field of view.
- The seeing in the whole atmosphere without the dome contribution as measured from the 2.1-mT, has a median value of  $0''.71$ .
- The temporal autocorrelation of the turbulence factors  $J_{h_l;h_u}$  (see § 3.2.3) shows that  $C_N^2$  evolves sensibly more slowly in the layers below 16 km (above see level) than in the layers above that altitude. The time lag corresponding to a 50% decorrelation is approximately equal to 2 and 0.5 hours for turbulence below and above 16 km, respectively. The longer the decorrelation time, the higher the potential performances of adaptive-optics observations are and the easier would be the development of multiconjugate adaptive optics systems. Rapid evolution of the  $C_N^2$  in the highest layers is in principle a negative behavior. However, this is counterbalanced by the very low  $C_N^2$  values in those layers. Further investigations will include the temporal correlation of the isoplanatic angle, which would integrate both effects.

From the GS data obtained during the 2000 campaign, a statistical analysis of the velocity of the turbulence layers has been made. The principal results and conclusions are the following:

- No evident general correlation between the  $C_N^2$  value in a layer and the layer speed has been found. The correlation is only evident during one night, in which  $C_N^2$  and  $\mathbf{V}$  values around 12 km are extremely high. This fact might indicate that only for  $\mathbf{V}$  values higher than a certain threshold level, the  $C_N^2$  value is correlated to the  $\mathbf{V}$  value. Further investigation is needed to prove or disprove this conjecture.
- The fastest layers are found between 10 and 17 km, with median speed value of  $24.4 \text{ m s}^{-1}$ . The layers above 17 km go notably more slowly (median speed of  $9.2 \text{ m s}^{-1}$ ), which is a positive feature for adaptive optics, because the wavefront deformations introduced by those layers would be corrected to a better degree than the lower layers, resulting in a wider field of view.

- The wavefront coherence-time for an ideal full-correction adaptive optics system has a median value of 6.5 ms.

Of particular interest are studies of the potential performances of multiconjugate adaptive optics systems for Extremely Large Telescopes (ELT). These studies can be carried out with the data set of paired  $C_N^2$  and  $\mathbf{V}$  profiles. For example, one can optimize the number of actuators and the temporal frequency of the different deformable mirrors for a required size of the corrected field of view. From the results obtained in this work, a qualitative guess is that a deformable mirror conjugated at 12 km would need less actuators but be faster than a deformable mirror conjugated at ground level.

The  $C_N^2$  and  $\mathbf{V}$  profiles are extremely important for the choice of the site for an ELT or any optical telescope with adaptive optics. The studies performed at the OAN-SPM have revealed that the site has truly excellent turbulence conditions. However, a longer-term monitoring is desirable, in order to confirm our results and identify seasonal behaviors, which is the motivation of developing a GS at UNAM.

We are grateful to the OAN-SPM staff for their valuable support. This work was done in the framework of a collaboration between the Instituto de Astronomía of the Universidad Nacional Autónoma de

México and the UMR 6525 Astrophysique, Université de Nice-Sophia Antipolis (France), supported by ECOS-ANUIES grant M97U01. Funding was also provided by the grants J32412E from CONACyT, IN118199 from DGAPA-UNAM, and the TIM project (IA-UNAM).

## REFERENCES

- Avila, R., Vernin, J., & Cuevas, S. 1998, *PASP*, 110, 1106
- Avila, R., Vernin, J., & Masciadri, E. 1997, *Appl. Opt.*, 36, 7898
- Avila, R., Vernin, J., & Sánchez, L. 2001, *A&A*, 369, 364
- Azouit, M., & Vernin, J. 2005, *PASP*, 117, 536
- Cruz, D., et al. 2003, *RevMexAA (SC)*, 19, 44
- Kisler, R., et al. 2001, *Bull. Am. Meteo. Soc.*, 82, 247
- Masciadri, E., Avila, R., & Sánchez, L. 2002, *A&A*, 382, 378
- \_\_\_\_\_. 2004, *RevMexAA*, 40, 3
- Masciadri, E., & Garfias, T. 2002, *A&A*, 366, 708
- Mason, B., Wycoff, G., & Hartkopf, W. I. 2002, <http://ad.usno.navy.mil/wds>
- Muñoz-Tuñón, C., Varela, A., & Vernin, J. 1992, *A&AS*, 125, 183
- Racine, R. 1996, *PASP*, 108, 372
- Roddier, F., Gilli, J., & Lund, G. 1982, *J. Opt. (Paris)*, 13, 263
- Sánchez, L., et al. 2004, *RevMexAA (SC)*, 19, 23
- Sarazin, M., & Roddier, F. 1990, *A&A*, 227, 294
- Tokovinin, A., Baumont, S., & Vasquez, J. 2003, *MNRAS*, 340, 52

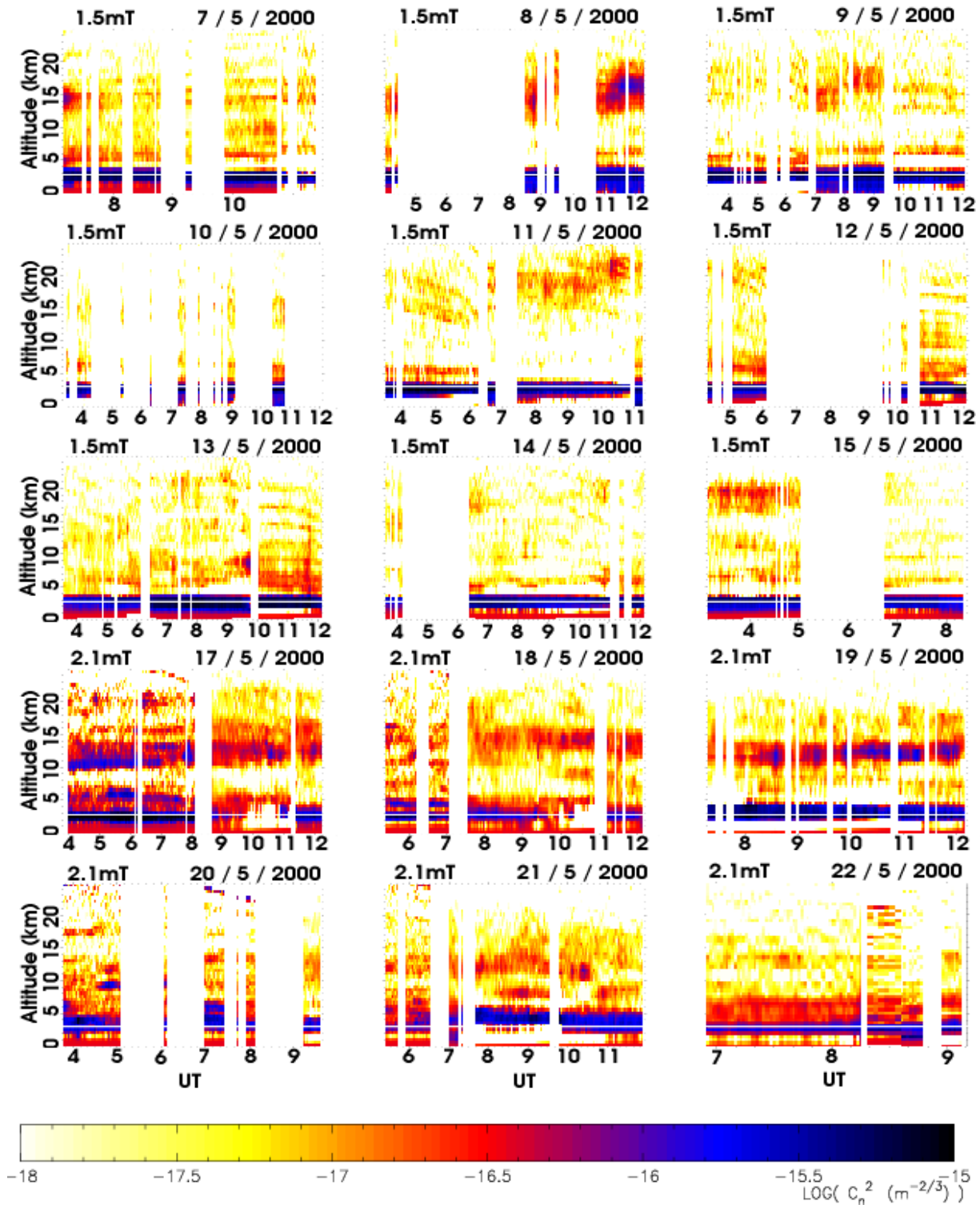
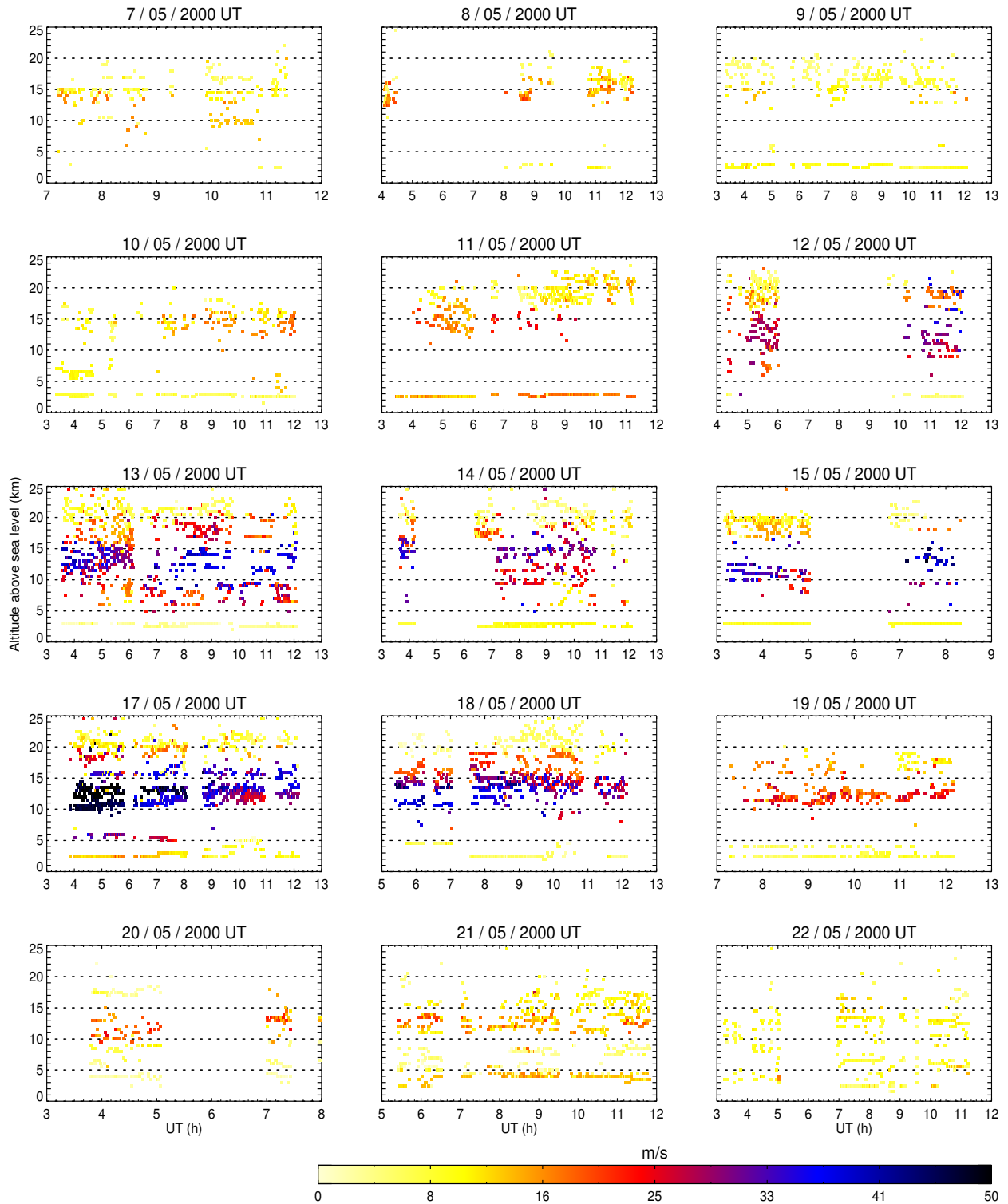


Fig. 1. Mosaic of the turbulence profiles measured during the whole campaign. Each box corresponds to one night. The vertical and horizontal axis represent the altitude (in km) above sea level and the universal time (in hours), respectively. The  $C_n^2$  values are coded in the color scale shown on the right-hand side of each box. The three upper rows and the two bottom rows contain the profiles obtained at the 1.5-mT and 2.1-mT, respectively. Time increases in the left-right and up-down directions. The white line centered at 2.8 km indicates the observatory altitude.



© 2007: Instituto de Astronomía, UNAM - Workshop on Astronomical Site Evaluation  
 Ed. Irene Cruz-Gonzalez, Juan Echevarria, & David Hiriart

Fig. 8. Mosaic of the wind profiles measured during the whole campaign. Each box corresponds to one night. The vertical and horizontal axes represent the altitude above sea level (observatory altitude: 2850 m) and the Universal Time, respectively. The wind speed values are coded with the color scale shown at the bottom. The three upper rows and the two bottom rows contain the profiles obtained at the 1.5-mT and 2.1-mT, respectively.